

# PCCP

Accepted Manuscript



This is an *Accepted Manuscript*, which has been through the Royal Society of Chemistry peer review process and has been accepted for publication.

*Accepted Manuscripts* are published online shortly after acceptance, before technical editing, formatting and proof reading. Using this free service, authors can make their results available to the community, in citable form, before we publish the edited article. We will replace this *Accepted Manuscript* with the edited and formatted *Advance Article* as soon as it is available.

You can find more information about *Accepted Manuscripts* in the [Information for Authors](#).

Please note that technical editing may introduce minor changes to the text and/or graphics, which may alter content. The journal's standard [Terms & Conditions](#) and the [Ethical guidelines](#) still apply. In no event shall the Royal Society of Chemistry be held responsible for any errors or omissions in this *Accepted Manuscript* or any consequences arising from the use of any information it contains.

Cite this: DOI: 10.1039/c0xx00000x

www.rsc.org/xxxxxx

ARTICLE TYPE

## Morphological and structural behavior of TiO<sub>2</sub> nanoparticles in the presence of WO<sub>3</sub>: crystallization of the oxide composite system

Anna Kubacka,<sup>a</sup> Ana Iglesias-Juez,<sup>a</sup> Marco di Michiel,<sup>b</sup> Ana Isabel Becerro,<sup>\*c</sup> and Marcos Fernández-García<sup>\*a</sup>

<sup>5</sup> Received (in XXX, XXX) Xth XXXXXXXXX 20XX, Accepted Xth XXXXXXXXX 20XX  
DOI: 10.1039/b000000x

Composite TiO<sub>2</sub>-WO<sub>3</sub> oxide materials were prepared by a single pot microemulsion method and studied during calcination treatments under dry air in order to analyze the influence of tungsten in the behavior of the dominant titania component. To this end, the surface and bulk morphological and structural evolution of the solid precursors was studied using X-ray diffraction and infrared spectroscopy. In the calcination process, differences in the dominant titania component behavior appeared as a function of the W/Ti atomic ratio of the precursor. First, the crystallization of the anatase phase is affected by tungsten through and effect in the primary particle size growth. Furthermore, such an effect also influences the anatase to rutile phase transformation. The study provides evidence that the W-Ti interaction develops differently for low/high W/Ti atomic ratio below/above 0.25 affecting fundamentally the above mentioned anatase primary particle size growth process and the subsequent formation of the rutile phase and showing that addition of tungsten provides a way to control morphology and phase behavior in anatase-based oxide complex materials.

### Introduction

Titanium dioxide (TiO<sub>2</sub>) is one of the most broadly applied oxides.<sup>1</sup> In fact, TiO<sub>2</sub> is the base of a significant number of materials with industrial applications related to catalysis among which the selective reduction of NO<sub>x</sub> in stationary sources,<sup>2,3</sup> and photocatalysis for pollutant elimination<sup>4,5</sup> or organic synthesis,<sup>6,7</sup> appear as rather important. Additional applications include its use as a white pigment in paintings,<sup>8</sup> as part of photovoltaic devices,<sup>9</sup> gas sensors,<sup>10,11</sup> high-refractive optics,<sup>12</sup> or as a food additive,<sup>13</sup> in cosmetics<sup>14</sup> and as a potential tool in cancer treatment.<sup>15</sup> In the catalytic applications already mentioned, titania is normally present in its thermodynamically stable nano-polymorph (i.e. anatase) and frequently used in combination with other oxides. In particular the use of tungsten oxide (WO<sub>3</sub>) finds utilization in all the catalytic fields above mentioned.<sup>1-7,16</sup>

However, relatively little is known about how the presence of tungsten oxide may alter the morphological and structural properties of the anatase phase. As anatase phase stability as well as chemical properties in the nanometer range are related, among a series of variables, to primary particle size,<sup>1,5,17</sup> the control of the nanostructure of this oxide appears as a basic objective in the optimization of the industrial-oriented properties of materials containing anatase. Understanding the crystallization process of anatase from amorphous solid materials typically obtained at the initial synthesis step appears of prime importance in this context. In a more general view, results for titania are also important in that they elucidate the general way in which primary particle size

and more generally speaking morphology can affect behavior of oxide materials.

Although the anatase crystallization process has been frequently analyzed in liquid phase,<sup>18,19,20,21,22,23</sup> it is less frequent the study of the solid-state transformation of amorphous titania materials into crystalline ones by thermal processes. This is however a rather common step in industrially relevant titania systems.<sup>1-7</sup> Due to thermodynamic issues, upon heating amorphous Ti-containing nano-materials would initially transform on anatase.<sup>24</sup> Exarhos et al. were the first to study the kinetics of the corresponding transition of amorphous films supported on silica substrates.<sup>24</sup> In other studies, using sol-gel<sup>25,26,27</sup> or microemulsion<sup>28,29</sup> procedures, details of the solid-state transformation mechanism leading to the anatase phase have been reported. Quantitative analysis of the key kinetic parameters controlling the amorphous titania to anatase transformation has been attempted in liquid media under hydrothermal conditions<sup>19</sup> and for solid-solid transformations concerning titania films,<sup>24,30</sup> powders,<sup>26,28,29</sup> or mesostructured<sup>31</sup> systems. The physical characteristics of the transformation (e.g. onset, reaction rate, energy of activation of the process) in air should be different from that in liquid media as, obviously, dissolution steps are critically involved in the latter. The broad range of temperatures where amorphous titania solids transform into anatase (see below) also tells of a wide range of situations within the air-assisted transformation occurring in solid materials. In fact, crystallization has been considered to be controlled either by surface<sup>24,28,31</sup> or interface<sup>26</sup> nucleation processes or limited by diffusion events in the case of dimensionally restricted (e.g.

films) structures.<sup>30</sup> Moreover, unexpected thermodynamic variables related to structural local order at the amorphous phase have been shown to play a role in controlling morphological properties.<sup>29,32</sup> As a first, naive approach to the rationalization of the nucleation mechanism, one may expect that either diffusion controlled or interface nucleation can work at low temperature, starting from the lowest onset published at ca. 350 °C, while the surface dominated mechanism may get primacy above certain temperature, ca. 600 °C.<sup>33</sup>

To our knowledge the situation is significantly less explored when titania is in contact with other oxide phase and the thermal treatment triggers the crystallization of both phases from amorphous precursors. The presence of a few surface modifiers such as silica<sup>34</sup> or bulk doping agents of anatase such as sulphur or iron<sup>35,36</sup> has been investigated. As said previously, we want to explore the crystallization phenomenon while titania is in contact with growing quantities of tungsten oxide and focus on how the morphology and structure of the titania is modified and can be controlled during a thermal treatment. At the same time the surface composition of the solid is followed using diffuse reflectance infrared fourier spectroscopy (DRIFTS) with the analysis of hydroxyl entities.<sup>28,29</sup> This intends to check in a simple way the changes occurred at the surface of the materials. To this end, we make use of in-situ synchrotron Hard X-ray (86.8 keV) diffraction and DRIFTS<sup>37</sup> techniques applied at different stages of the amorphous to anatase and further to rutile transformation(s) of materials synthesized with a microemulsion method.

## Experimental Section

### Preparation of the TiO<sub>2</sub> oxide precursors.

Materials were prepared using a single pot microemulsion preparation method using *n*-heptane (Scharlau) as organic media, Triton X-100 (Aldrich) as surfactant and hexanol (Aldrich) as cosurfactant. A TiO<sub>2</sub> reference sample was obtained as a first step using a microemulsion with acetic acid (to fix the initial pH to a value of 5.0) into the aqueous phase and titanium tetraisopropoxide as precursor. In all composite samples and the WO<sub>3</sub> reference, ammonium tungsten oxide (Alfa Aesar) was introduced in the aqueous phase of a microemulsion. After 30 min of agitation, a stoichiometric (to obtain the corresponding W(VI) hydroxide) quantity of tetramethylammonium-hydroxide (TMAH) was introduced from the aqueous phase of a similar microemulsion. For nanocomposite samples, after 5 min of contact and pH adjustment with acetic acid (pH 5), titanium tetraisopropoxide was introduced into the previously resulting microemulsion drop by drop from a mixture with isopropanol (2:3). Water/Ti and water/surfactant molar ratios were, respectively, 110 and 18 for all samples.<sup>38,39</sup> The resulting mixture was stirred for 24 h, centrifuged, and the separated solid precursors rinsed with methanol and dried at 110 °C for 12 h. After drying, the solid precursors were subjected to a heating ramp (2 °C min<sup>-1</sup>) up to 750 °C, maintaining this temperature for 2 h. Samples names are Ti/W for the titania/wolframia references, and xWTi for the composite ones where x refers the molar content of WO<sub>3</sub> (for example, 01 is a 0.1 molar percentage of the

tungsten oxide in relation to a fixed amount of titania corresponding to 1 mol).

### Characterization experiments.

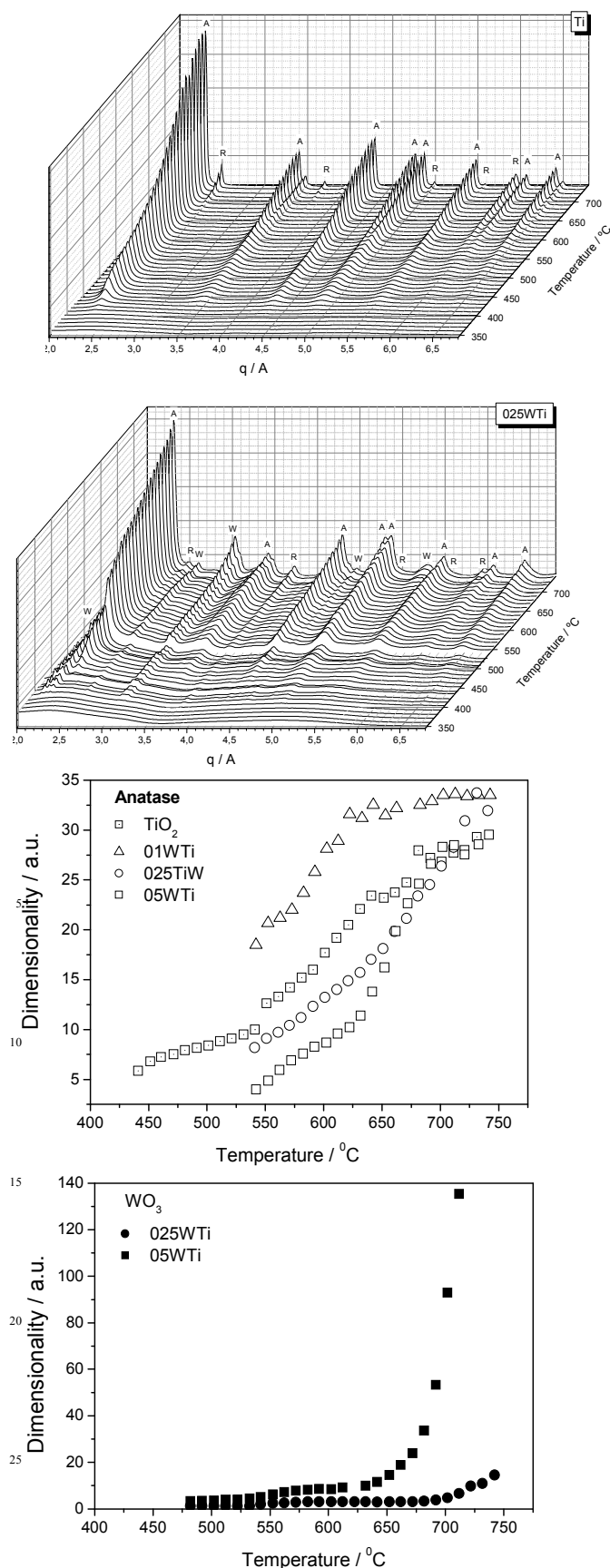
Time-resolved hard X-ray diffraction (TR-XRD) data were collected at beamline ID15B (86.8 keV,  $\lambda = 0.143 \text{ \AA}$ ,  $\Delta E/E \sim 1.4 \times 10^{-3}$ ) using a digital flat-panel X-ray detector (Trixel Pixium 4700).<sup>40</sup> Calibration of the X-ray wavelength was made using a NIST LaB<sub>6</sub> powder. In the TR-XRD experiments dealing with the thermal evolution of titania nanomaterials, the sample (ca. 10 mg) was kept in a 1 mm quartz capillary of 0.1 mm wall thickness and heated from 25 to 750 °C with a ramp of 3 °C min<sup>-1</sup> under a 20 % O<sub>2</sub>/He using a modified version of a plug-flow reactor system due to Chupas et al.<sup>41,42</sup> A chromel-alumel thermocouple, inserted directly into the sample bed, was used to measure the temperature of the sample. The plug-flow geometry ensures a perfect gas contact with the solid, eliminating any problem from oxygen supply to the system. Two dimensional powder patterns were collected in less than 40 seconds with the sample located at less than 1 mm from the thermocouple, without measurable temperature gradient along the sample bed. In such conditions and as demonstrated in previous works, the error in the (average) temperature measurement during a complete XRD scan is less than 2 °C.<sup>42</sup> The powder diffraction rings were subsequently radially integrated after applying geometrical and x-ray polarization corrections. The patterns were analyzed using the Rietveld method<sup>43</sup> with the TOPAS software (TOPAS version 4.2, Bruker AXS 2009). Refined parameters were: background coefficients, zero error, scale factors, unit cell parameters, and weight percent of phases. Starting parameters for anatase, tungsten oxide (monoclinic) and rutile phases were taken, respectively, from Howard et al.,<sup>44</sup> Vogt et al.,<sup>45</sup> and Murugesan et al.<sup>46</sup>

Diffuse Reflectance Infrared Fourier Transform Spectra (DRIFTS) were taken in a Bruker Equinox 55 FTIR spectrometer fitted with an MCT detector. The DRIFTS cell (Harrick) was fitted with CaF<sub>2</sub> windows and a heating cartridge that allowed samples to be heated to 600 °C. Samples of ca. 60 mg were dried *in situ* at 110 °C under 20 % O<sub>2</sub> in He and ramped at 3 °C min<sup>-1</sup> up to 600 °C. The spectra consisted of 100 accumulations with a total of 1 min acquisition time, using a 4 cm<sup>-1</sup> resolution.

## Results and Discussion

### a) Phase behavior during thermal treatment

The thermal evolution of the initially amorphous materials under the O<sub>2</sub>/He atmosphere was investigated with the combined use of TP-XRD (temperature programmed XRD) and DRIFTS techniques. **Fig. 1/ Fig. S1** show the raw diffraction data obtained for each sample investigated. The amorphous structure of the initial materials only displays broad, diffuse-like features of variable intensity in the first patterns of all samples. The materials develop into two phases corresponding to the TiO<sub>2</sub> anatase structure (PDF 04-07-0701 (ICDD, 2013), corresponding to the *I41/amd* space group) and the WO<sub>3</sub> monoclinic structure (PDF 01-083-0951 (ICDD, 2013), corresponding to the *P21/n* space group). As detailed below, minor contributions of other titania phases (brookite, rutile) are occasionally observed. In fact brookite is detected below 1% in all catalyses.



30 Fig. 1. From top to bottom: Representative XRD patterns of the Ti reference and 025WTi sample under a  $O_2/He$  temperature ramp. Anatase

(A), Rutile (R), and  $WO_3$  (W) peaks are marked. Volume analysis of anatase and  $WO_3$  (monoclinic) phases. See text for details

35 Differences among samples concern the nascent phases onset as well as thermal evolution. The single titania reference allows visualizing the anatase evolution from ca. 420  $^{\circ}C$  in presence of a rather modest rutile contribution which becomes increasingly important above ca. 670  $^{\circ}C$ . Comparison with xWTi samples is  
 40 illustrated in the two lower panels of Fig. 1. The dimensionality parameter obtained from Rietveld analysis for the anatase phase is presented for doing such comparison in qualitative terms.<sup>47</sup> The 1WTi sample is not included as anatase is a relatively minor phase, difficult to analyze, and the  $WO_3$  phase displays  
 45 dimensionality values above 1000 nm (not obtained with confidence). The effect of tungsten in the anatase phase onset seems clear and roughly equal for all xWTi samples (delay of ca. 110 K). Above the onset, the influence of tungsten appears strongly dependent on the W/Ti atomic ratio. This will be  
 50 quantitatively analyzed below. Concerning the  $WO_3$  monoclinic phase, Fig. 1 evidences a drastic effect of titania on the stabilization of such phase as far as the W content is low and oxide-oxide interface interaction can play a role.

The information related to the titania polymorphs evolution as  
 55 resulted from the Rietveld analysis is summarized in Fig. 2. For 01WTi and 025WTi samples, anatase is detected as a dominant phase (rutile and brookite below 1%) in presence of growing quantities of the monoclinic  $WO_3$  phase that are, however, only barely visible in the 01WTi case (Fig. 1). The evolution of the  
 60 anatase to rutile transformation is thus limited by the presence of tungsten in the composite system for these two samples, while it is more clearly detected for the two other samples (05WTi and 1WTi) as clarified in the plot presented in Fig. 2.

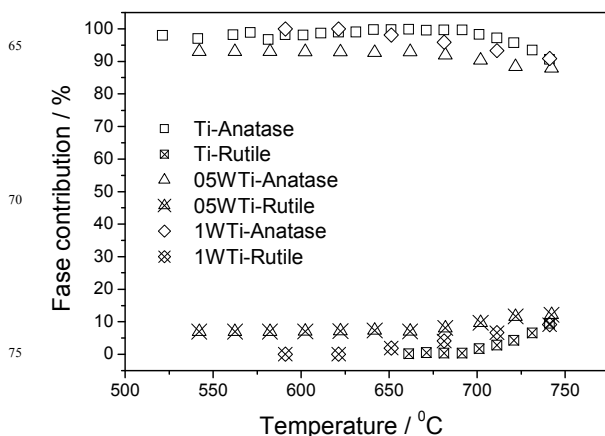


Fig. 2. Titania phase distribution for Ti reference and WTi samples.  
 80 Phases below 1 % are not included. 01WTi and 025WTi are not displayed in the plot due to the fact that anatase is the single, dominant titania phase (above 98 %). Note, however, that rutile peaks are visible in Fig. 1 for all W-Ti samples.

85 As expected in titania samples, rutile is more clearly observed at high temperature (above 600  $^{\circ}C$ ) but always with a moderate contribution to the titania phase distribution. The evolution of rutile seems to suggest that tungsten presence may affect differently the anatase behavior at high and low content.  
 90 Inhibition of rutile growth below 750  $^{\circ}C$  is observed in the 01WTi while the others samples retard the growth of this phase

with respect to the Ti reference.<sup>48</sup> This is likely related or at least connected to the control of anatase primary particle size as discussed below. On the other hand, the monoclinic WO<sub>3</sub> phase is also observed from relatively low temperature, above 400 °C, and for all composite samples although the percentage of WO<sub>3</sub> detected by XRD in the 01WTi composition is very low.

### b) Mechanism of anatase crystallization

The anatase crystallization mechanism was investigated in detail for selected samples with XRD during isothermal treatments. **Fig. 3** shows, as an example, the XRD patterns of the 025WTi sample recorded with time at three different temperatures (400 °C, 410 °C and 420 °C). We analyzed the intensity change of the largest (101) anatase peak as a function of treatment time at several temperatures per sample. Many solid state phase transitions have been studied using the Avrami-Erofeev formalism.<sup>24,28,30,31</sup> Hancock and Sharp<sup>49</sup> derived the following equation from which the kinetic parameters of the crystallization of a solid-state reaction can be extracted:

$$\ln(-\ln(1-\alpha)) = \ln(K) + m \ln(t) \quad (1)$$

where  $\alpha$  is the fraction isothermally crystallized at time  $t$ ,  $K$  is the rate constant and  $m$  is an exponent independent of temperature but responsive to the nature of the nucleation (and growth) and to the geometry of the particles. Typically,  $m$  values ca. 0.5 indicate that the rate is limited by diffusion, around 1.0-1.5 a zero order, first-order or a phase boundary controlled mechanism, between 2 to 3 if the nucleation controls the rate (typically mentioned as bulk control), and above 3 when nucleation is affected by presence of pores.<sup>24,28,30,31,49</sup>

**Table 1.** Nucleation and Growth mechanism parameters for Ti reference and W-Ti samples:  $m$  parameter of the equation 1 and activation energies (kJ mol<sup>-1</sup>) for the processes described in equation 1 ( $E_{HS}$ ) and 2 ( $E_D$ ). Standard errors of the observables are presented in parenthesis.

Sample	$m$	$E_{HS}$	$E_D$
Ti	3.25(0.26)	95(31)	10.9(3.5)
01WTi	-	-	55.4(5.0) / 11.3(3.8)
025WTi	3.11(0.23)	115(25)	30.6(3.7) / 16.0(4.0)
05WTi	-	-	17.8(4.1)

The results of the analysis using equation 1 for selected samples are summarized in **Table 1**. Corresponding experimental data sets are shown in **Fig. 4**. The analysis of the nucleation mechanism yielded  $m$  values close to 3 indicating a bulk controlled mechanism. A number of different anatase samples rendered values either close to 1<sup>28,30,31,50</sup> or 3.<sup>50</sup> All of these  $m$  values have been observed in nano-materials but values of 1 are typically interpreted as a surface controlled mechanism, characteristic of nanosized materials. Differences in the  $m$  values may be related to the networking or boundary conditions between the initial nuclei. Particularly, the addition of acetic acid as a pH controller but also as a potential capping agent seems critically affecting networking/boundary conditions in our Ti reference; in absence of this agent the pure reference produced using the same microemulsion method renders a value of 1.<sup>28</sup> The study is thus indicating that the nucleation and growth process is strongly affected by this pH-controller/chelating agent. In any case and considering the result of the composite sample studied, it seems

that the presence of tungsten does not alter significantly the behavior of the pure Ti reference system.

The dimensionality of the anatase primary particle has been also frequently analyzed within the Sharp-Hancock framework.<sup>51</sup> Data in **Table 1** indicate relatively small differences among xWTi samples with respect to the titania reference. As will be further detailed using a surface sensitive technique (infrared), single oxide anatase displays a particle with elongated shape, favoring a rice-type grain morphology.<sup>28,29</sup> Such morphology seems to suffer limited changes in presence of tungsten.

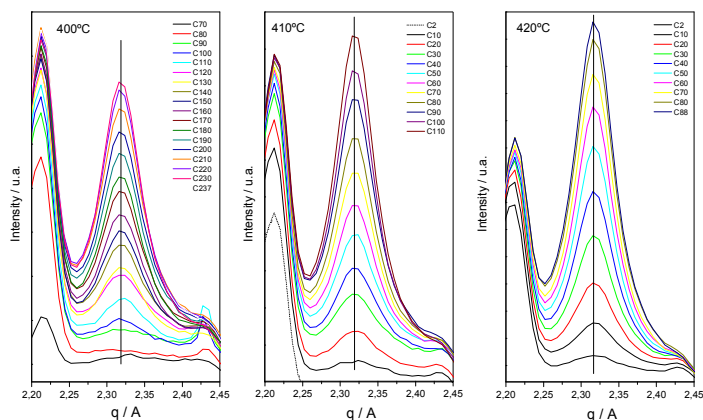


**Fig. 3.** Selected XRD patterns around the (101) anatase reflection vs. time for a representative example (025WTi sample) under isothermal conditions.

The Arrhenius plot (**Fig. 5**) obtained from isothermal treatment data allows the calculation of the activation energy of the process. Values of the activation energy are rather similar and equal within experimental error. Relatively low values have been consistently observed in the literature, going from ca. 70<sup>50</sup> to ca. 140<sup>24,28,31</sup> kJ mol<sup>-1</sup>; although values above 200 kJ mol<sup>-1</sup> were obtained in other cases.<sup>28,30</sup> Recent studies suggest that structural different connecting details among the titania building TiOx ( $x=4-7$ ) block units present in the amorphous materials can be at the origin of these differences. This has obtained both experimental<sup>29</sup> and theoretical<sup>52</sup> support although it is still an open question. In any case, in our case the activation energy values presented in **Table 2** reinforce the idea that the presence of tungsten affects minimally the nucleation and growth process initial steps of the anatase phase.

A mild effect is however observed in subsequent steps related to the primary particle growth. From sufficiently larger particles and assuming an isotropic diffusion-limited coarsening, Lifshitz, Slyozov and Wagner<sup>53,54</sup> developed a rigorous mathematical approach to Ostwald ripening which provides the time evolution of an ensemble of particles. According to the theory, the coarsening kinetics are given by:

$$D^n - D_0^n = K t \quad (2)$$

where  $D$  is the average particle size of the growing particle at time  $t$  and  $K$  is the rate constant. The exponent can provide insights on the mechanism of the nanocrystal growth and has values between 1 and 4 but it has been always fixed to 2 in the case of anatase.<sup>28,30,31,36</sup> In the present case 2 is also the best

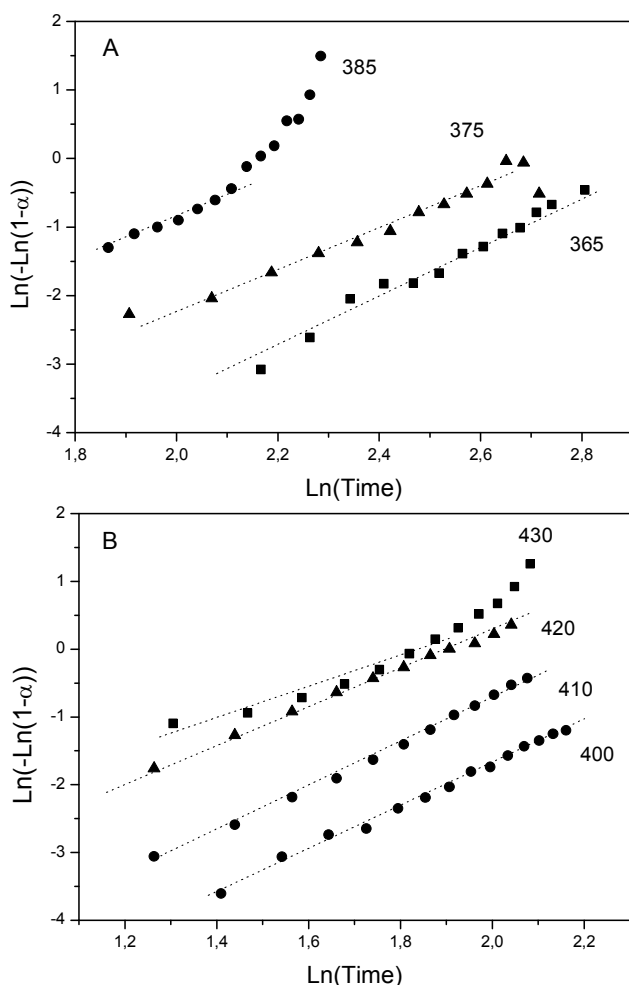


Fig. 4. Sharp- Hancock plots (equation 1) for the T (A) and 025WTi (B) samples. Numbers indicates the temperature ( $^{\circ}\text{C}$ ) of the isothermal treatment. Linear fittings are presented as dotted lines.

option as judged by fitting results. As shown in **Fig. 5** the systems behave similarly except in the 01WTi case where two regions of linear behavior are detected. A similar behavior may be also present in the 025WTi samples but it is clearly less obvious. The “classical” behavior of Ti and 05WTi samples indicates that their anatase particle growth could be described by a Ostwald ripening process. This does not appear the case of the other two xWTi samples (see below). In such cases, two activation energy values are presented in **Table 1**. Values between ca. 15 to 30  $\text{kJ mol}^{-1}$  are consistent with the majority of results reported in the literature and attributed to a growth process dominated or strongly influenced by the dehydration of initially formed anatase surface layers.<sup>28,30,31,36,55</sup> In the present case, we detected a modest growing trend with the increasing content of tungsten, a fact that might be indicative of an increasing importance of a preferential orientation growth with W content.<sup>36</sup>

More important is the presence of two well differentiated regions in the 01WTi material and, less markedly, in 025WTi. This indicates that these systems do not follow an isotropic diffusion-limited Ostwald-type coarsening (required for equation 2) and may be interpreted as if in this case we can have a restricted coarsening model. Grain or particle growth process

progresses quickly until it encounters a stopper. As this only occurs in the 01WTi case and to a rather modest level in 025WTi, the interpretation seems complex. It appears that a specific tungsten to titanium contact at surface layers promotes (anatase) primary particle size growth until the contact between the anatase and  $\text{WO}_3$  phases is diminished, presumably by aggregation at high temperature. After such point the “normal” anatase behavior is recovered as suggested by the energy of activation values obtained. Such observations would suggest that tungsten interaction with titania does not profoundly alter anatase nucleation but may have an effect in the anatase primary particle size growth in the cases where a different initial interaction is achieved. As said, this leads to an increase of anatase primary

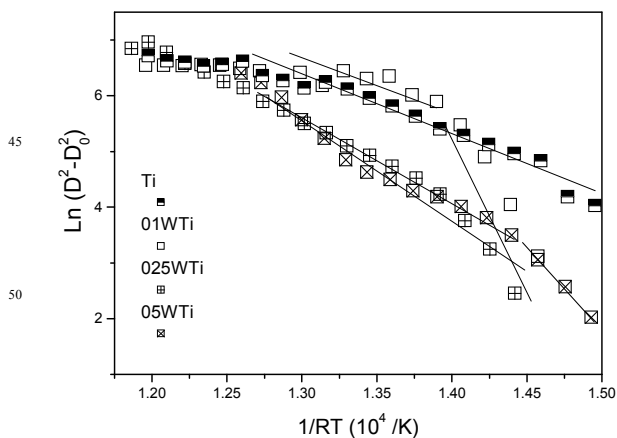


Fig. 5. Arrhenius-type plot showing the anatase phase nucleation process temperature dependence as measured with XRD data for Ti and 025WTi samples. Linear fittings are shown as solid lines.

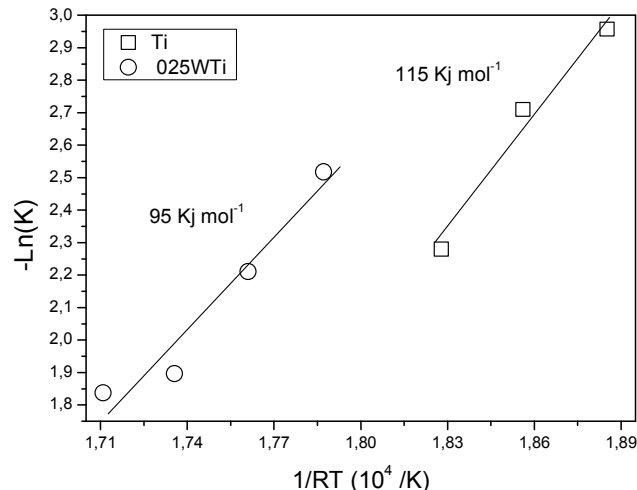


Fig. 6. Arrhenius-type plot showing the temperature dependence of the anatase primary particle size growth as measured using XRD data. Linear fitting are shown as solid lines. See text for details.

particle size in the 01WTi sample. Restricting anatase primary particle size growth is effectively attained only in samples with high W/Ti atomic ratio (above a 0.25 W/Ti ratio), in turn suggesting that the 025WTi sample is a boundary below/after which the surface interaction between the two metals is modified as an effect of the extent of the interface and/or a change in the nature of the interaction (i.e. change in surface tungsten species present at anatase surface). As detailed above, the way tungsten

affects anatase particle size for “high” loading samples is related to a more hindered dehydration of surface layers during the growth step of the anatase primary particle. This slows the growth process of the anatase primary particle size.

### c) Analysis of macrostrain of the anatase unit cell

The unit cell parameters and volume of the main phases detected by XRD during the O<sub>2</sub>/He ramp are displayed in Fig. 7. The monoclinic WO<sub>3</sub> component displays a reasonable similar behavior among samples although subtle differences are

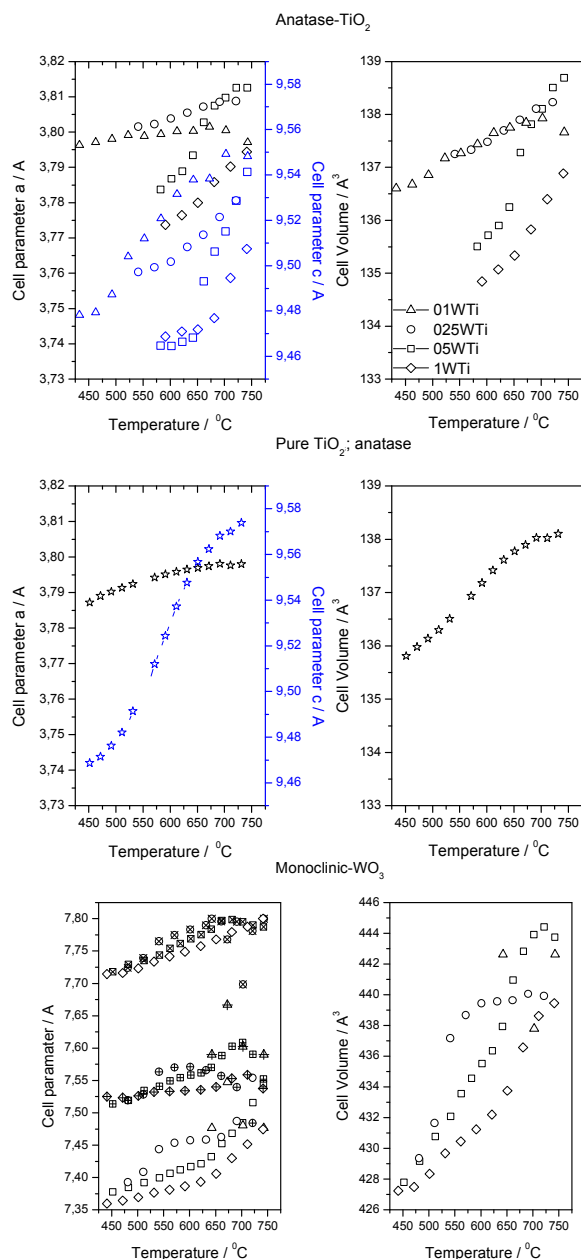


Fig. 7. Cell parameters and volume for the anatase-TiO<sub>2</sub> (a,c) and monoclinic-WO<sub>3</sub> (a<b<c) phase as obtained from Rietveld analysis of XRD data taken during an O<sub>2</sub>/He temperature ramp. The Ti reference system is presented in separated plots.

encountered in the *c*-parameter and cell volume. In the case of anatase, the main subject of this contribution, the results

corresponding to the WTi materials can be compared with the single Ti reference. As previously observed for the nucleation and growth process, we observed a differential behavior between the W-low content samples (particularly 01WTi) and the remaining ones. Such different behavior is more acute in results corresponding to the cell volume and *a* cell parameter than for the *c* cell parameter, although it is detected in all cases. This fact is more clearly observed in Fig. 8 where the macrostrain (*S*) at the *a*- and *c*-axes was calculated according to:

$$S = 100 \times (p_i - p_{\text{final}}) / p_{\text{final}} \quad (3)$$

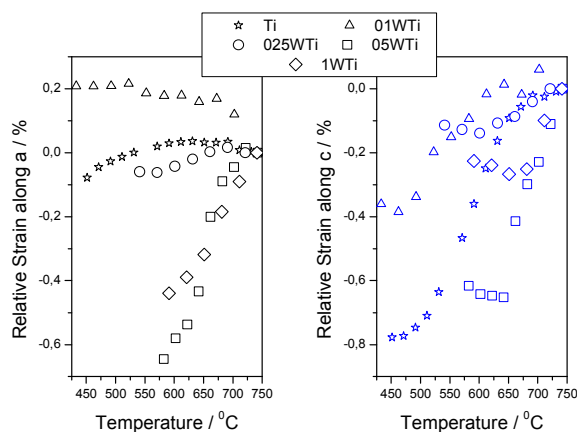


Fig. 8. Evaluation of the strain present in the anatase unit cell during a O<sub>2</sub>/He temperature ramp. Thermal effects eliminated as described in the text. Strain is defined as  $(p_i - p_{\text{final}}) / p_{\text{final}} \times 100$ , where *p* is the corresponding anatase cell parameter.

where *p<sub>i</sub>* is the parameter at temperature *T* and *p<sub>final</sub>* is the parameter at the highest *T* of this study (750 °C). For these calculations, we eliminated the thermal effect of the parameters using the data obtained with a nanosized anatase reference system (details at the supporting information file). Strain evolution vs. temperature appears significant in the two cell parameters.

Interestingly, a negative strain is always observed for the *c*-parameters while positive/negative strain is observed in the case of the *a* parameter for 01WTi / the rest of W-Ti samples. The Ti reference and the 025WTi sample only showed rather modest strain values in the last case. While the absolute values of the data presented in Fig. 8 may be affected by a significant number or error sources, the qualitative trend indicates that tungsten affects anatase in two different ways. Being the 025WTi sample borderline for different behavior, the low tungsten sample (01WTi) is the only one that presents positive strain in the *a* parameter.

The macrostrain characteristics of anatase have been found to vary considerably depending on a significant number of physico-chemical variables. In particular, three effects are believed to play a role in determining crystal behavior of nanometer size oxides; i) the positive pressure exerted by the increasing curve surface as primary particle size becomes smaller and will tend to compress the structure, thus generating a negative macrostrain. The strength

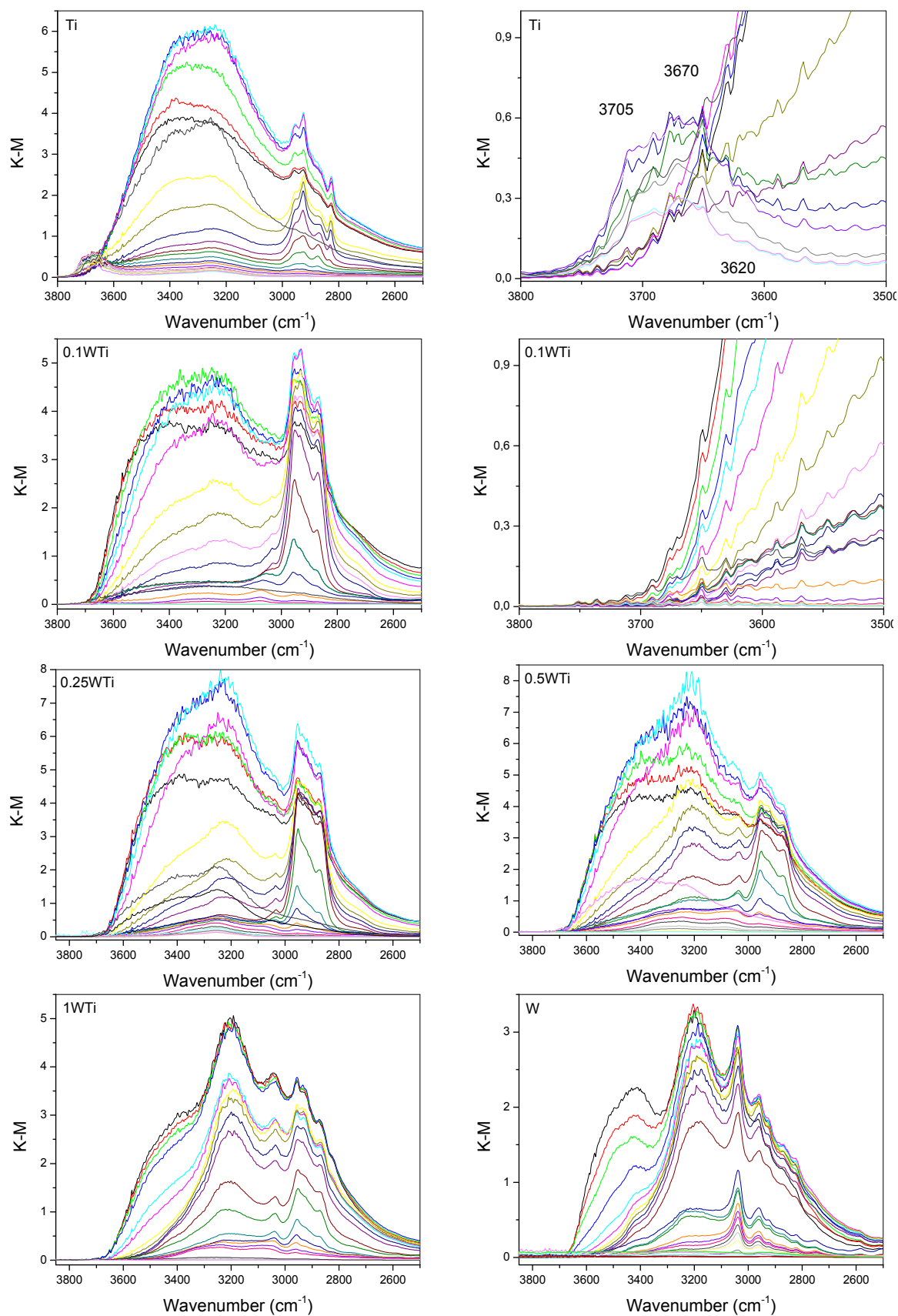


Fig. 9. IR spectra of the Oh region for the WTi and Ti reference samples under a O<sub>2</sub>/He temperature ramp. Spectra at RT and each 25 degrees from 50 to 550 °C are presented. Color codes: black RT; red 50 °C; green 75 °C; blue 100 °C; cyan 125 °C; magenta 150 °C; yellow 175 °C; dark yellow 200 °C; navy 225 °C; purple 250 °C; wine 275 °C; Olive 300 °C; dark cyan 325 °C; royal 350 °C; orange 375 °C; violet 400 °C; pink 425 °C; white 450 °C; light gray 475 °C; gray 500 °C; light yellow 525 °C; light cyan 550 °C; dark gray RT. For selected samples an expanded view of the isolated hydroxyl region is presented

of this effect is related to the surface chemistry and is a consequence of basic surface energy considerations.<sup>22,56</sup> Second ii), the curvature effect can be counterbalanced by the generation of surface dipoles from surface Ti-dangling bonds coordinated to water in the first hydration shell.<sup>55</sup> Water distorts Ti coordination, generating parallel dipoles perpendicular to the crystalline surface and repelling each other, thus creating a negative pressure on the particle (positive strain). Finally iii), the third macrostrain effect is caused by defects in the anatase structure which also produce a negative pressure on small crystallites.<sup>57</sup> With one effect predicting compression in both directions, one effect predicting expansion on both directions and one effect predicting expansion along *c* and contraction in the *a,b*-plane, different outcomes are possible.

Positive/negative macrostrain for *a/c* axes with larger effect on the *c* axis suggests that the effect of curvature and/or vacancies dominates over dipole effect. This has been previously observed in other samples.<sup>58,59</sup> Here this behavior is only observed in the case of the 01WTi sample and the most characteristic point with respect to the other W-Ti samples is the *a* axis positive macrostrain which would indicate a promoting influence of tungsten in defect number at the anatase phase for this specific sample. The behavior of the Ti reference and the majority of the remaining samples (i.e. 01WTi excluded) seems to be dominated by a large negative macrostrain along the *a* and *c* axes indicating a larger concentration of defects and a more pronounced effect of the curvature,<sup>50,60</sup> both facts related to the lower anatase particle size with respect to the 01WTi sample (and the Ti reference).

The presence of tungsten is thus affecting significantly the anatase nucleation and growth process by controlling anatase primary particle size after nucleation though an effect in the hydration of the surface layer with significant consequences in the structural properties of the W-Ti composite samples. The study of the macrostrain is reflecting differences among samples having low/high W/Ti atomic ratio as a result of the anatase particle size and pointing out to a different nature/number of defects in both situations.

#### d) Analysis of the surface of anatase particles: Infrared study

To further analyze the influence of tungsten presence in the composite samples, we carried out an infrared analysis of the hydroxyl region. The evolution of hydroxyl infrared signals is connected to the dehydration process taking place during the thermal treatment in O<sub>2</sub>/He and, moreover, provides information about the surface of the materials.<sup>28,29,36,61,62,63,64</sup> The latter is mostly related to the presence of isolated OH entities with characteristic wavenumbers above ca. 3550 cm<sup>-1</sup>. For the Ti reference, the expanded view included in Fig. 9 allows exploring this issue. Three bands at ca. 3620 (tailing contribution reflecting (101)-type surface terminations), 3670 (also (101)-terminated surfaces) and 3705 (in this case (100)-terminated surfaces) cm<sup>-1</sup> were observed.<sup>29,36,61,62</sup> This is common in anatase materials having elongated particle shapes along the *c* axis and exposing mainly (101) and (100) surfaces. Interestingly, the expanded view of the 01WTi sample indicates that all these isolated hydroxyl species are lost when tungsten is present. Maybe a small contribution around 3620 cm<sup>-1</sup> may still persist with rather low intensity. While the absence of isolated hydroxyl at temperatures

above ca. 200 °C is typical for monoclinic WO<sub>3</sub>,<sup>65</sup> this is not the case of anatase materials.<sup>28,29,36,61,62</sup> This indicates that the surface of anatase is strongly interacting with the other oxide counterpart in composite materials up to modify the local neighborhood and alter drastically the corresponding vibrational frequencies. The reasons for the latter are unknown as it may imply a strong interaction with other hydroxyls, up to a level not present in anatase, and/or the elimination of such species from the surface. Independently of the reason, the influence of tungsten in anatase surface is clearly demonstrated and justified the differences observed in the dehydration process above discussed in sections b/c.

The bands corresponding to interacting hydroxyl species and loosely bond water molecules are also presented in Fig. 9. The most representative ones are located above 3000 cm<sup>-1</sup> as below the presence of residual C-H stretching contributions makes assignment rather complex.<sup>28,29,36,64</sup> The comparison with a monoclinic WO<sub>3</sub> reference indicates that the most characteristic hydroxyl bands at ca. 3235 and 3425 cm<sup>-1</sup>, assigned respectively to water and interaction hydroxyls,<sup>65</sup> dominate the spectrum and likely the surface exposed to the atmosphere for samples having a tungsten content equal or above 025WTi. The complete analysis of the infrared spectra indicates that the 01WTi sample maintains a singular behavior, likely as an effect of an exalted interaction between components and achieved in a significant less degree for the remaining composite samples. This agrees with the conclusions of the XRD study.

## Conclusions

In this work we analyzed the evolution of complex Ti-W oxide systems from their solid precursor state. To this end, four composite samples having increasing tungsten content (from 0.1 to 1 molar content with respect to 1 mol of titanium) and the corresponding single metal oxide references were synthesized using a microemulsion method.

The surface and bulk morphological and structural behavior of amorphous precursors during thermal treatments was studied with the help of high energy X-ray diffraction and infrared spectroscopy. The thermal behavior and evolution of complex tungsten-titania oxide-based composite materials do not display a simple relationship with the W/Ti atomic ratio of the material, showing two well differentiated regions below/above a 0.25 atomic ratio.

Focusing in the titania behavior, the study provides evidence that the presence of tungsten would thus produce different effects as a function of the W/Ti atomic ratio. For W/Ti values above 0.25, the analysis evidences a significant influence in anatase phase growth steps leading a more easy control of the anatase primary particle size. W also influences the thermal evolution of the anatase component by delaying the rutile phase appearance and/or limiting its contribution to the titania phase distribution with a complex dependence on the W/Ti atomic ratio, which in turn is likely related to the evolution of the anatase primary particle size.

The study provides thus evidence that control of anatase behavior through contact with tungsten is thus possible and seems intimately connected with the evolution of anatase surface layers in the growth step and subsequent effects in anatase primary

particle size and titania phase distribution during thermal treatments.

### Acknowledgements

Anna Kubacka and Ana Iglesias-Juez thank the MINECO for 5 Postdoctoral “Ramón y Cajal” Fellowships. Work at the “Instituto de Catálisis y Petroleoquímica (CSIC)” was carried out with financial support from CICYT (project CT2010-14872/BQU). Work at the “Instituto de Ciencia de Materiales de Sevilla” was carried out with financial support from Junta de 10 Andalucía (FQM6090) and CSIC (201460E005). Authors are indebted to ESRF for provision of beamtime at ID15.

### Notes and references

- <sup>a</sup> Instituto de Catálisis y Petroleoquímica, CSIC, C/Marie Curie 2, 15 Cantoblanco, 28049-Madrid, Spain. Fax: +34 91 5854760; Tel: +34 91 5854939; E-mail: m.fernandez@icp.csic.es
- <sup>b</sup> ESRF; 6 rue Jules Horowitz; 38043-Grenoble CEDEX (France).
- <sup>c</sup> Instituto de Ciencia de Materiales de Sevilla, CSIC-Universidad de Sevilla, C/Américo Vespucio 49, 41092-Sevilla, Spain. Fax: +34 95 20 4460165; Tel: +34 95 4489545; E-mail: anieto@icmse.csic.es
- † Electronic Supplementary Information (ESI) available: analysis of thermal expansion coefficient of the anatase phase. See DOI: 10.1039/b000000x/
- 1 M. Fernández-García, A. Martínez-Arias, J.C. Hanson J.A. Rodriguez, *Chem. Rev.* 2004, **104**, 4063.
  - 2 H. Bosh, F. Janssen, *Catal. Today*, 1988, **2**, 369.
  - 3 P. Forzatti, *Catal. Today*, 2000, **62**, 51.
  - 4 M.R. Hoffman, S.T. Martin, W. Choi, D.W. Bahneman, *Chem. Rev.* 1995, **95**, 69.
  - 5 A. Kubacka, M. Fernández-García, G. Colón, *Chem. Rev.*, 2012, **112**, 1555.
  - 6 A. Maldoti, A. Molinari, R. Amadeni, *Chem. Rev.* 2002, **102**, 3811.
  - 7 L. Palmisano, V. Augugliaro, M. Bellardita, A. Di Paola, E. García-López, V. Loddo, V. Marci, G. Palmisano, S. Yurdakal, *ChemSusChem*, 2011, **4**, 1431.
  - 8 R.W. Johnson, E.S. Thieles, R.H. French, *Tappi. J.*, 1997, **80**, 233.
  - 9 A. Hagfeld, M. Gratzel, *Acc. Chem. Res.*, 2000, **33**, 269.
  - 10 „Gas sensors“, G. Sheviglieri (Editor), Kluwer, Dordrecht, 1992.
  - 11 D. Morris, R.G. Edgell, *Chem. Mater.*, 2001, **11**, 3207.
  - 12 J.S. King, E. Graungnard, *Adv. Mater.*, 2005, **17**, 1010.
  - 13 L.G. Phillips, D.M. Barbeno, *J. Dairy Sci.*, 1997, **80**, 2726.
  - 14 H. Selhofer, *Vacuum Thin Films*, (August, 1999) 15.
  - 15 A. Fujishima, X. Zhao, D.A. Tryk, *Surf. Sci. Rep.*, 2008, **63**, 515.
  - 16 M.J. Muñoz-Batista, A. Kubacka, R. Rachwailk, B. Bachiller-Baeza, M. Fernández-García, *J. Catal.*, 2014, **309**, 428.
  - 17 “Synthesis, Properties and Applications of Solid Oxides” J.A. Rodríguez and M. Fernández-García (Eds.). John Wiley, New York, 2007. Chpt. 4, 5, 20.
  - 18 K. Yanagisawa, J. Ovenstone, *J. Phys. Chem. B*, 1999, **103**, 7781.
  - 19 H. Yin, X. Wadax, T. Kitamura, S. Kanbe, S. Murasawa, H. Mori, T. Sakata, T. Yamagida, *J. Mater. Chem.*, 2001, **11**, 1694.
  - 20 A. Testino, I.R. Bellobono, V. Buscaglia, C. Canevali, M. D’Arienzo, S. Polizzi, R. Scotti, F. Morazzoni, *J. Am. Chem. Soc.*, 2007, **129**, 3564.
  - 21 M.P. Finnegan, J.F. Banfield, *Chem. Mater.*, 2008, **20**, 3443.
  - 22 V. Jensen, M. Bremholm, N. Lock, G.R. Deen, T.R. Jensen, B.B. Iversen, M. Niederberger, J.S. Pedersen, H. Birkedal, *Chem. Mater.*, 2010, **22**, 6044.
  - 23 A. Jagminas, G. Niaura, J. Kuzmarskyte-Jagminiene, V. Pakštas, *Solid State Sci.*, 2013, **26**, 97-104.
  - 24 G.J. Exarhos, M. Aloi *Thin Solid Films* 1990, **193**, 42.
  - 25 B. Ohtani, Y. Ogawa, S. Wishimoto, *J. Phys. Chem. B*, 1997, **101**, 3746
  - 26 H. Zhang, J.F. Banfield, *Chem. Mater.*, 2002, **14**, 4145.
  - 27 G. Lee, J.M. Zuo, *J. Am. Ceram. Soc.*, 2004, **87**, 473.
  - 28 M. Fernández-García, X. Wang, C. Belver, J.C. Hanson, J.A. Rodríguez, *J. Phys. Chem. C*, 2007, **111**, 674.
  - 29 M. Fernández-García, C. Belver, J.C. Hanson, X. Wang, J.A. Rodríguez, *J. Am. Chem. Soc.*, 2007, **129**, 13604.
  - 30 S.Y. Choi, M. Mamak, S. Speakman, N. Chopra, G.A. Ozin, *Small*, 2005, **2**, 226.
  - 31 B.L. Kirsch, E.K. Richman, A.E. Riley, S.H. Tolbert, *J. Phys. Chem. B*, 2004, **108**, 12698.
  - 32 A. Kubacka, A. Iglesias-Juez, A. Martínez-Arias, M. Di Michiel, M.A. Newton, M. Fernández-García, *ChemCatChem*, 2012, **4**, 725.
  - 33 H. Zhang, J.F. Banfield, *J. Phys. Chem. C*, 2007, **111**, 6621.
  - 34 A. Li, Y. Jin, D. Muggli, D.T. Pierce, H. Aranwela, G.K. Brockman, J.X. Zhao, *Nanoscale*, 2013, **5**, 5854-5862.
  - 35 S. Tieng, R. Azouani, K. Chlor, A. Kanaev, *J. Phys. Chem. C*, 2011, **115**, 5244.
  - 36 K.C. Christoforidis, A. Iglesias-Juez, S.J.A. Figueroa, M. Di Michiel, M.A. Newton, M. Fernández-García, *Phys. Chem. Chem. Phys.*, 2012, **14**, 5628.
  - 37 M.G. O’Brien, A.M. Beale, S.D.M. Jacques, M. Di Michie, B.M. Weckhuysen, *Appl. Catal. A*, 2011, **311**, 468.
  - 38 P.G. De Gennes, C. Taupin, *J. Phys. Chem.*, 1982, **86**, 2294.
  - 39 A. Kubacka, M. Fernández-García, G. Colón, *J. Catal.*, 2008, **254**, 272.
  - 40 J.E. Daniels, M. Drakopoulos, *J. Synchrotron Rad.*, 2009, **16**, 463.
  - 41 P.J. Chupas, K.W. Chapman, C. Kurtz, J.C. Hanson, P.L. Lee, C.P. Grey, *J. Appl. Cryst.*, 2008, **41**, 822.
  - 42 S.J.A. Figueroa, et al.; *J. Appl. Crystallog.* 2013, **46**, 1523.
  - 43 H.M. Rietveld, “A profile refinement method for nuclear and magnetic structures”. *J. Appl. Crystallogr.*, 1969, **2**, 65-71.
  - 44 C.J. Howard, T.M.; Sabine, F. Dickson, *Acta Crystallogr.*, 1991, **B47**, 462-468.
  - 45 T. Vogt, P.M. Woodward, B.A. Hunter, *J. Solid State Chem.*, 1999, **144**, 209-215.
  - 46 M. Murugesan, P. Kuppusami, E. Mohandas, *Mater. Res. Bull.*, 2010, **45**, 6-8.
  - 47 Dimensionality parameter is presented to provide (exclusively) a qualitative trend due to its high error at the initial steps of the nucleation and growth process.
  - 48 L. J. Alemany, M. A. Larrubia, M. C. Jiménez, F. Delgado, J. M. Blasco, *React. Kinet. Catal. Lett.* 1997, **60**, 41.
  - 49 J.D. Hancock, J.H. Sharp, *J. Am. Ceram. Soc.*, 1972, **55**, 74.
  - 50 J.R. Eltzoltz, C. Tyrsted, K.M.O. Jensen, M. Bremholm, M. Christensen, J. Becker-Christensen, B.B. Iversen, *Nanoscale* 2013, **5**, 2372.
  - 51 F.S. Hulbert, *J. Britih Ceramic Soc.* 1969, **6**, 11.
  - 52 A. Bruin, S. Consta; T.-K. Sham, *J. Phys. Chem. C*, 2011, **115**, 22257.
  - 53 C.Z. Wagner, *J. Phys. Chem.* 1901, **37**, 385.
  - 54 I.M. Lifshitz, V.V. Slyosov, *J. Chem.Phys. Sol.*, 1961, **19**, 35.
  - 55 G. Li, L. Li, J. Boerio-Goates, B.F. Woodfield, *J. Am. Chem. Soc.*, 2005, **127**, 8659.
  - 56 D.A. Porter, K.E. Easterling, M.Y. Sherif, *Phase transformation in metals and alloys*, CRC Press, Boca Raton, USA, 2004.
  - 57 I.E. Grey, N.C. Wilson, *J. Solid State Chem.*, 2007, **180**, 670.
  - 58 V. Swamy, D. Menzies, B.C. Muddle, A. Kuznetsov, L.S. Dubrovinsky, Q. Dai, V. Dmitriev, *Appl. Phys. Lett.*, 2006, **88**, 243103.
  - 59 M.I. Ahmad, S.S. Bhattacharya, *Appl. Phys. Lett.*, 2009, **95**, 191906.
  - 60 H.Z. Zhang, B. Chen, J.F. Banfield, *Phys. Chem. Chem. Phys.*, 2009, **11**, 2553.
  - 61 M. Digne, P. Sauet, M. Breysse, H. Touthoat, *J. Catal.*, 2002, **211**, 1.
  - 62 S. Dzwigaj, C. Arrouvel, M. Breysse, C. Geantet, S. Inoue, H. Touthoat, P. Raybaud, *J. Catal.*, 2005, **236**, 245.
  - 63 K.J.A. Raj, B. Viswathan, *ACS Appl. Mater. Interfaces*, 2009, **1**, 2462.
  - 64 C. Lamberti, A. Zecchina, E. Groppo, S. Brodiga, *Chem. Soc. Rev.*, 2010, **39**, 4951.
  - 65 S.M. Kana, Z. Lu, J.K. Cox, G. Bernhardt, C.P. Tripp, *Langmuir*, 2002, **18**, 1707.